Journal of Materials Science Research and Reviews

8(4): 39-71, 2021; Article no.JMSRR.73077

Bending Behavior of Ferrocement Composite Semi Circular Light Weight Panels for Roof Construction

Yousry B. I. Shaheen[1], Zeinab A. Etman[1,2] and Labiba A. Marzouk[3*]

[1]Department of Civil Engineering, Faculty of Engineering, Menoufia University, Egypt.
[2]Department of Civil Engineering, Higher Institute of Engineering and Technology, Menoufia, Egypt.
[3]Department of Civil Engineering, Higher Institute of Engineering and Technology, Tanta, Egypt.

Authors' contributions

This work was carried out in collaboration among all authors. All authors read and approved the final manuscript.

Article Information

Editor(s):
(1) Prof. Pradip K. Bhowmik, University of Nevada Las Vegas, United States.
(2) Dr. Yong X. Gan, California State Polytechnic University, USA.
Reviewers:
(1) Ibuchim Bobo Cyril-Ogunkah, University of Westminste, United Kingdom.
(2) Abdulhaq Hadi Abedali, Mustansiriyah University, Iraq.
Complete Peer review History: https://www.sdiarticle4.com/review-history/73077

Original Research Article

Received 27 June 2021
Accepted 07 September 2021
Published 11 September 2021

ABSTRACT

This paper will presents the results of research to study to demonstrate the structural performance integrity of ferrocement composite semicircular lightweight panels for roof construction. This proposed panels are lighter in weight relative to the conventional reinforced concrete panels. The sandwich panels consisted of two thin ferrocement layers reinforced with one or two layers of closely spaced welded wire mesh. The core of the panel was made of light weight fibrous foam concrete. The steel meshes were tied by steel wires of the two skin layers together and to act as shear connectors to transfer shear between the two ferrocement skin layers through the core in-between. The thickness of the ferrocement skin layer was 25 mm. The core material will be 70 mm thick which consisted of pyrite and ad pour 55 as lightweight aggregate. Two types of the steel mesh were used to reinforce the ferrocement skin layers. Namely: welded wire mesh and expanded metal mesh. Steel wire shear connector will be used to tie the top and bottom ferrocement skin layers through lightweight concrete in between and to provide shear reinforcement. Experimental investigation was conducted on the proposed panels. A total of 16 sandwich semicircular panels having the dimensions of 500 mm in width, and 2000 mm. in length will be tested under four lines loadings of span 1900 mm up to failure. The deformation characteristics and cracking behavior

**Corresponding author: E-mail: labiba.marzouk@yahoo.com;*

were measured and observed for each panel. The results obtained will be compared with theoretical ones by using Abaqous finite elements program version 14. The results will show that high ultimate and serviceability loads, crack resistance control, high ductility ratio and good energy absorption properties could be achieved by using the proposed panels. This could be of great construction advantages for both developed and developing countiess alike

Keywords: Ferrocement, Arch, Abaqus, Slab.

1. INTRODUCTION

The American Concrete Institute [1] has defined Ferrocement material as a type of reinforced concrete commonly constructed of hydraulic cement mortar reinforced with closely spaced layers of relatively small wire diameter mesh. The mesh maded of metallic or other suitable materials.

Shaheen and Eltahawy [2] presents a new precast U-shape ferrocement forms that reinforced with various types of metallic and non-metallic mesh reinforcement. The experimental program make comparison casting and testing ten slabs having the total dimensions of 500x100x2500 mm incorporating 40 mm thick U shape permanent ferrocement forms. The result of the experimental program showed that high ultimate and serviceability loads, better crack resistance control, high ductility, and good energy absorption properties could be achieved by using the proposed slabs and low cost compared with control specimen.

Shaheen, Y., Eltaly, B. and Abdul-Fataha, S. [3], compared numerical models and designed an experimental program to investigate the structural behaviour of twelve ferrocement beams under three point loadings up to failure. They compared the twelve beams that different of the types of reinforcement: steel bars, traditional wire meshes, and welded and expanded wire meshes. The results of the numerical models and experimental tests showed that the beam with fiberglass meshes gives the lowest first crack load and the maximum load. Their results concluded further that the ferrocement beam reinforced with four layers of welded wire meshes had the best structural behaviour than those beams reinforced with other types of wire meshes.

The effect of the strength of ferrocement jackets for initially damaged exterior RC beam-column joints is presented by [4]. In this study, the experimental observation noticed an improvement in the ultimate load, yield load carrying capacity with increase in stiffness of the ferrocement-jacketed joints in comparison with the control joint.

Ramakrishnan et al. [5] studied the flexural strength and behavior of steel box girders for precast purposes. Through partial cement replacement (link) at different rates of silica fume (SF) (0-25% in grades 5%), the casting iron bar Trunking to ascertain whether there is an increase or decrease in the compressive strength and tensile strength because of the addition SF.

From the results of compressive and split tensile strength, it was found that 10% of the SF6 replacement produced higher strength. After obtaining the optimum proportion of fine grouting, iron box girders with SF (10% SF with 90% cement), two without SF and two steel girders of iron cement are cast and tested for bending, under two point loading with two layers of wire mesh. The bending strength of the iron box girder without fine grouting is compared with that of a cement iron steel beam. The test results indicated that the decrease in the bending strength of the beam with voids is less compared to the solid beam due to the lower self-weight of the hollow box beam.

Abbas et al. [6] studied the bending behavior of high-strength hollow concrete girders taking into account different volume depressions. 14 solid and hollow reinforced concrete beams were tested under four-point bending to evaluate the bending behavior of hollow concrete beams. The experimental program demonstrated two main variables: volume reduction ratio and steel fiber inclusion. Ten hollow girders with square center holes of rib lengths of 60, 80 and 100 mm in addition to four solid girders were fabricated to evaluate the test parameters. These beams are reinforced with either 1% steel fibres or no fibres at all.

Considering the experimental work, analytical equations were introduced to evaluate the faulting and peak loads of the hollow beams. And after testing it was found that the ductility of the hollow beam with a volume reduction of 16% and 28.4% was higher than that of the reference solid beam, while the ductility of the hollow beam with

a volume reduction of 44.4% was completely similar to that of the solid beam. In addition, the stiffness values for the hollow beams were 19 to 37% higher than that of the reference solid beam. Based on the results obtained, the results showed that hollow reinforced concrete beams with 1.0% steel fiber and with a size reduction up to 44.4% could replace the solid beams without experiencing a significant decrease in strength, ductility and toughness.

Yang et al. [7] made a study in a new mechanical model of Ferritic Reinforced Polyvinyl Cement Fiber Composite (PVA-RFCC), using PVA fibers and steel wire mesh (SWM). A series of experiments were conducted to study its mechanical properties, and a comparative analysis was also performed to evaluate the flexural strength.

The experimental results showed that the bending strength of the PVA-RFCC samples was significantly increased compared to the PVA-ECC (PVA-engineered cement composites) samples. The highest increases in initial hardness as well as crushing strength, displacement ductility modulus and hardness of PVA-RFCC samples were improved by 62.4%, 174.7%, 251.0% and 192.5%, respectively.

Nasser et al. [8] carried out laboratory experiments to study the effect of using different types of reinforcement on the bending behavior of steel hollow core plates with integrated PVC tubes. The samples, as indicated by the practical program, were twelve plates with dimensions 1100 x 400 x 55 mm. The effect of four different types of reinforcement was investigated in this study including; Steel wire mesh, macro and micro steel fibers or a combination of both, steel bars and CFRP bars.

The results showed that the slab reinforced with macro steel fibers had the highest bending resistance, while that reinforced with steel bars showed the highest stiffness and had the lowest deflection among all the tested panels. Also, the dry design density of all hollow core slabs was determined to be less than 2000 kg/m^3 which is within the requirements for lightweight concrete as defined by previous studies.

Applies b. Shaheen 1A, Hala Refaat and Ashraf Mohamed Mahmoud [9] the team conducted experiments to demonstrate the experimental and numerical performance of iron-concrete walls reinforced with welded steel mesh, expanded steel mesh, fiberglass mesh and Tensar mesh separately. The samples were twelve RC walls with dimensions of 450 mm x 100 mm x 1000 mm under concentric compressive loads. The studied variables are the type of reinforcing material, the number of mesh layers and the volume fraction of the reinforcement. The research aims to study the evaluation of the effect of using new innovative materials in strengthening RC composite walls. Study of nonlinear finite elements; (NLFEA) was implemented to simulate the behavior of composite walls using ANSYS-10.0 software. The parametric study is also described to study changes that can mainly affect the mechanical behavior of the model such as changing the wall dimensions. The numerical results obtained indicated the acceptable accuracy of FE simulation in estimating the experimental values. Also, the strength gained for samples reinforced with welded steel mesh was 40% higher compared to those reinforced with expanded steel mesh. Ferrocement specimens tested under axial compressive loads exhibit higher final loads and energy absorption capacity compared to conventional reinforced concrete specimens.

2. EXPERIMENTAL PROGRAM

The practical program was divided into two parts, the first stage related to reinforcement. The main objective was to study the mechanical properties of used steel and wire mesh. As for the second stage, the main objective was to study the final load and compare between the flexural behavior, the percentage of plasticity, the energy absorption, and the breakdown pattern when the control panels collapsed, reinforced with steel bars and reinforced steel plates. Expanded metal mesh, welded galvanized steel mesh, fiberglass mesh, structural steel bars with steel mesh and fiberglass mesh were used. Table 1 presents the details of the experimental program.

In this program, ten samples are illustrated, cast and tested to study their behavior under bending loads. Table 1 shows details of the experimental program for all test samples while Fig. 1 shows images of the reinforcement configurations for all panels. Fig. 2 confirms the types of mesh and polypropylene fibers used.

2.1 Materials

- The fine aggregate used in the experimental program was from natural siliceous sand. With features that meet E.S.S. specifications. 1109/2008. It was virtually free of impurities and clean with a

specific gravity of 2.6 t/m3 and a fineness modulus of 2.7.

- The cement used is the ordinary Portland cement produced by the cement factory in Suez. It conforms to the chemical and physical properties with the Egyptian Standard Specification E.S.4756-11 [10].
- Silica fume (S.F) has been used to enhance the strength of iron mortar and concrete core. It has been used as a partial by weight substitute for cement in mortar mixtures. It was S.F. The average particle size was 0.1 μm and the silicon dioxide content was 93%.
- Fly ash was used as a percentage of cement. Conforms to the chemical and physical requirements of ASTM C618 and relevant international quality standards for fly ash. The fly ash had a relatively low specific gravity and a fineness of 2.10 and 330 kg/ m 2, respectively.
- The water used was fresh, potable water free of impurities used for mixing and treating reinforced concrete and conforming to E.C.P. package testing. 203/2007.
- The superplasticizer used is HRWR High Range Water Reducer. It was used to improve the workability of the mix. The mixture used was produced by CMB GROUP under the trade name Addicrete BVF. Meets the requirements of ASTM C494 (Type A and F). The mixture is a thick brown liquid 1.18 kg/L at room temperature. The amount of HRWR was 1.0% of the weight of the cement.
- E300 polypropylene fibers were used. It has been used in concrete mixes to produce a fibrous concrete jacket to improve the properties of concrete. Conforms to ASTM C1116 [11]. The addition ratio of 900 g/m3 was selected based on manufacturing recommendations. Technical specifications and mechanical properties of E300 polypropylene fibers as shown by the producing company are shown in Table 2.
  Ref. no. [12-15] included Codes and specifications for the materials used, Experimenta program and Talking about the behavior of Structural of the ferrocement construction.
- Steel reinforcement. 8mm high tensile steel bars in the tension side and 8mm high tensile steel bars in the compression side whose resistive stress and maximum strength of the steel material were 551N/mm2 and 670 N/mm² was used for reinforced concrete reinforcement and Ferrocement box bridges for testing.
- Expanded steel mesh is used as reinforcement for iron cement beams. The technical specifications and mechanical properties of the expanded metal mesh as shown by the producing company are shown in Table 3 and shown in Fig. 2 and Table 3 Technical and Mechanical Properties of Expanded Metal Mesh [1].

Tabel 1. Types of meshes and fibres used

Specimens designation	Code of girder	Reinforcement wire mesh	Reinforcing main steel bars	
			Tens.	Comp.
1	S 1	Reinforced by conventional with fiber	6 Φ 6	6 Φ 6
	S 2	Reinforced by conventional without fiber	6 Φ 6	6 Φ 6
2	B3	Reinforced by two layers of welded steel mesh at each side	6 Φ 6	6 Φ 6
	S 4	Reinforced by three layers of welded steel mesh at each side	6 Φ 6	6 Φ 6
	S 5	Reinforced by four layers of welded steel mesh at each side	6 Φ 6	6 Φ 6
3		Reinforced by one layer of expanded steel mesh at	6 Φ 6	6 Φ 6
	S 6	each side.		
	S 7	Reinforced by two layers of expanded steel mesh at each side.	6 Φ 6	6 Φ 6
	S 8	Reinforced by one layer of expanded steel mesh at each side	6 Φ 6	6 Φ 6
4	S9	Reinforced by one layer of Tenax mesh at each side.	6 Φ 12	6 Φ 10
	S 10	Reinforced by two layers of Tenax mesh at each	6 Φ 6	6 Φ 6

side.

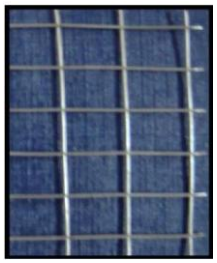

a) Welded steel mesh

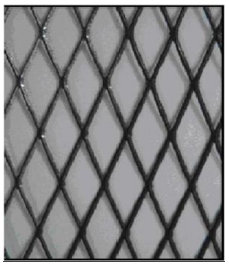

b) Expanded steel mesh

c) Fiber

d) Tenax mesh (LBO330)

Fig. 1. Types of meshes used in experimental program

Table 2. Chemical and Physical Properties of Fiber Mesh e300 [15]

Absorption	Nil
Specific Gravity	0.91
Fiber Length	Single cut
Electrical Conductivity	Low Electrical Conductivity
Acid & Salt Resistance	High Acid & Salt Resistance
Melt Point	324°F (162°C)
Thermal Conductivity	Low
Ignition Point	1100°F (593°C)

Table 3. Technical and mechanical properties of expanded metal mesh [1].

Style	1532
Sheet Size	1 m width × 10 m length
Weight	1.3 Kg/m2
Diamond size	16 × 31mm
Dimensions of strand	1.25 × 1.5mm
Proof Stress (N/mm2)	199
Proof Strain × 10-3	9.7
Ultimate Strength (N/mm2)	320
Ultimate Strain× 10-3	59.2

- **The Welded steel mesh** used was obtained from China, and it was used as reinforcement for ferrocement girders. The technical specifications and mechanical properties of welded steel mesh as provided by producing company are given in Table 4. It is comply with of ACI 549.1R-97 (2009).

- **TENAX LBO SAMP (330)** is polypropylene Geogrid especially for reinforcement applications. The Geogrid is manufactured from a unique process of extrusion and biaxial orientation to enhance their tensile properties It features consistently high tensile strength and modulus, excellent resistance to construction damages and environmental exposure. Properties of this mesh can be shown in Table 5.

Table 4. Technical and mechanical properties of welded metal mesh [1]

Dimensions	12.5mm × 12.5 mm
Weight	430 gm /m^2
Proof Stress	737 N/mm^2
Ultimate Strength (N/mm^2)	834 N/mm^2
Ultimate Strain × 10^{-3}	58.8
Proof Strain × 10^{-3}	1.17

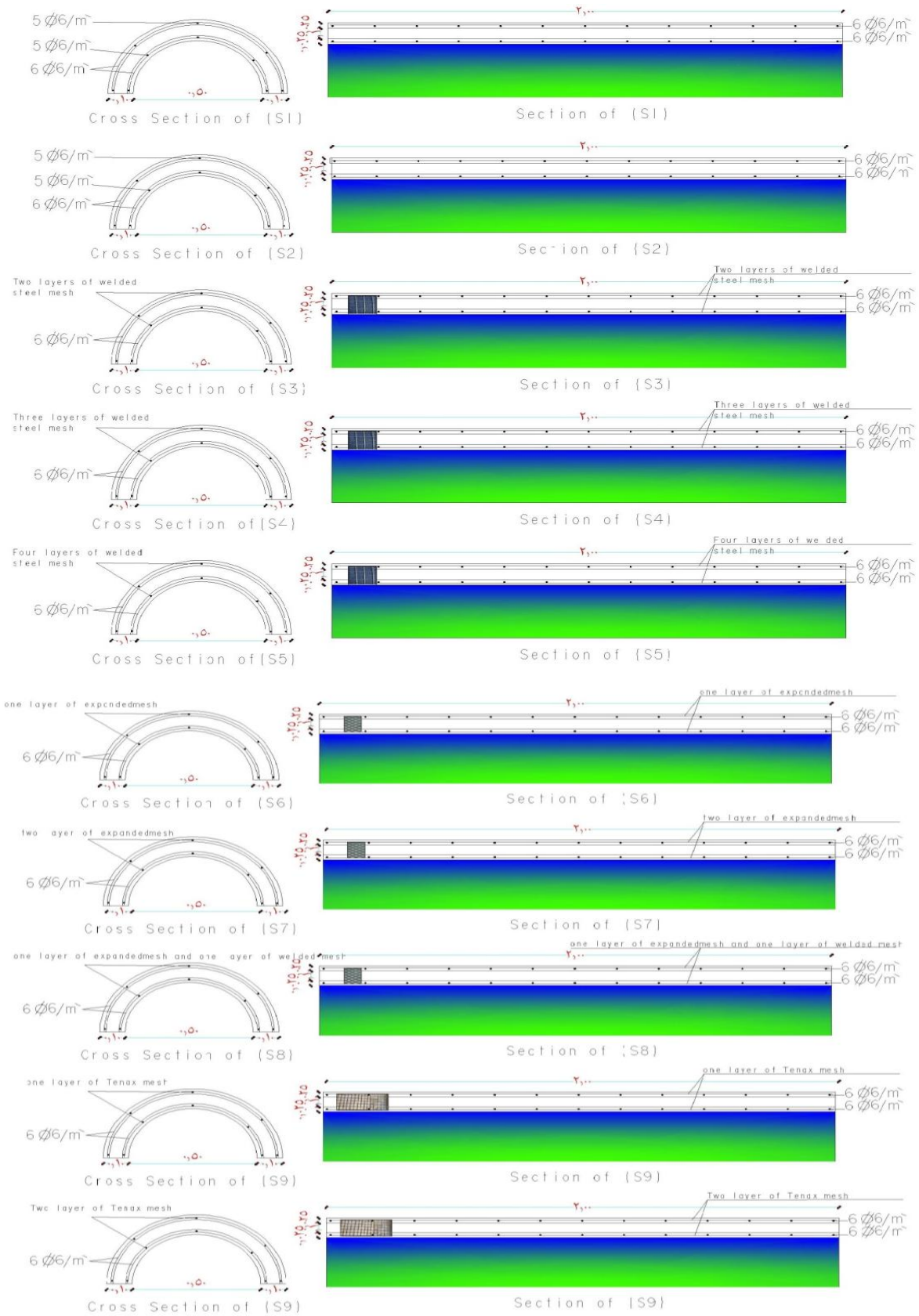

Fig. 2. Types of meshes and fibres used

Table 5. Physical characteristic of TENAX (LBO 330) from its data sheet

Structure	Biaxial geogrid
Mesh type	Rectangular apertures
Standard color	Black
Polymer type	Polypropylene
Carbon black content	2%
Dimensional characteristics	(LBO 330) Samp
Aperture size Md	40 mm
Aperture size Md	27 mm
Mass per unit area	420 g/m2
Roll width	4 m
Roll length	50 m
Roll diameter	.52 m
Roll volume	1.1 m3
Gross roll weight	137 kg

Fig. 3. Shows the modeling Expanded Metal mesh shape

Fig. 4. Shows the modeling

Fig. 5. Shows the modeling welded Metal mesh shape

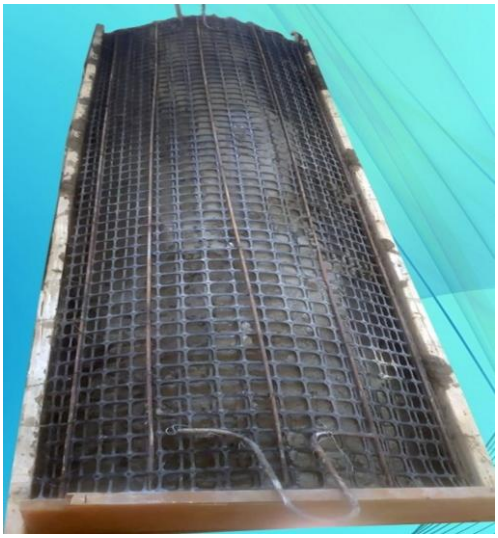

Fig. 6. Shows the modeling tenex mesh shape

2.2 Mortar Matrix

Cement mortar consists of sand, ordinary Portland cement, silica fume and fly ash. A key factor from the mix design was to determine how to partially replace a large amount of cement with silica fumes and fly ash to increase the strength of the slurry matrix without any adverse effects on the quality and properties of the mix in both the fresh and hardened state. A condition of good workability was essential, to allow the slurry matrix to penetrate through the layers of steel mesh reinforcing. A super plasticizing agent was used to increase the flow characteristics and speed up early strength development. Mortar mixtures for iron cement were made using a water/cement ratio of 0.35, and a superplasticizer of 2% by weight of cement, while sand/cement ratio of 2.0, 10% by weight of cement was replaced by SF and 20% by weight. The cement was replaced by fly ash and the percentage of adding fiber e300 was chosen to be 0.9 kg/m 3 8. The results showed that the average compressive strength of iron cement mortar after 28 days (fcu) was 35 MPa. For all mixtures, the materials were mechanically mixed in the laboratory with a mechanical mixer with a capacity of 0.05 m 3, as it was found that the volume of the mixed materials was within this range. The constituent materials were mixed first; Add the mixing water and re-mix the entire stain again in the blender. Mechanical pressure was applied to all samples. Iron cement sand-cement mortar consists of sand, ordinary Portland cement, silica fume and fly ash. The main purpose of the mix design was to determine how to partially replace a large amount of cement with silica fumes and fly ash to increase the strength

of the slurry matrix without any adverse effects on the quality and properties of the mix in both the fresh and hardened state. . A condition of good workability was essential, to allow the slurry matrix to penetrate through the layers of steel mesh reinforcing. A super plasticizing agent was used to increase the flow characteristics and speed up early strength development. Mortar mixtures for iron cement were made using a water/cement ratio of 0.35, and a superplasticizer of 2% by weight of cement, while sand/cement ratio of 2.0, 10% by weight of cement was replaced by SF and 20% by weight. The cement was replaced by fly ash and the e300 fiber addition percentage was chosen to be 0.9 kg/m3 8. The average compressive strength of iron cement mortar after 28 days (fcu) was found to be 35 MPa. For all mixtures, in vitro mechanical mixing with mechanical mixing with a capacity of 0.05 m3 was used, as it was found that the volume of the materials mixed was within this range. The constituent materials were mixed first; Add the mixing water and re-mix the entire stain again in the blender. Mechanical stress was applied to all samples as shown in Fig. 9.

Fig. 7. Shows the modeling welded Metal mesh shape

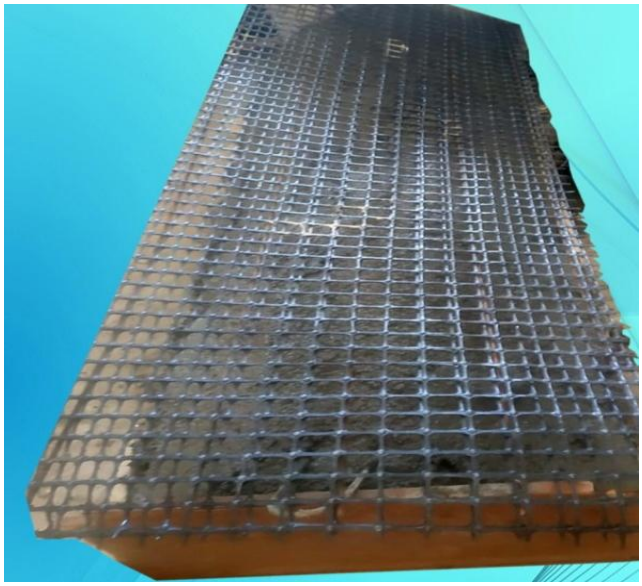

Fig. 8. Shows the modeling tenex mesh shape

Fig. 9. Shows the modeling during casting

2.3 TEST Setup

At the time of testing, the specimen was painted with white paint to facilitate the visual crack detection during testing process. A set of four demecll points was placed on one side of the specimen to allow measuring the strain versus load during the test. Demec points were placed as shown in Fig. 10. The specimens were tested on a testing loading frame with a four loading points. The span length was 1800 mm while the distance between the two loading points was 600 mm. dial gauges were used to measure deflection at mid span and under points of loading while strain gauges attached to the top and bottom of the surface of concrete at the critical sections to evaluate its behavior. All the values of deflection at the variable positions and top and bottom strain values were recorded. Cracks were traced throughout bottom of the specimen and then marked with black markers. The first crack-load of each specimen was recorded. The load was increased until complete failure of the specimen was reached. Test setup of specimen can be shown in Fig. 11 while Figs. 12-16 shows specimen during the test.

Fig. 10. Shows specimen during the test

Fig. 11. Shows specimen during the test

Fig. 12. Shows specimen during the test for S1

Fig. 13. Shows specimen during the test for S5

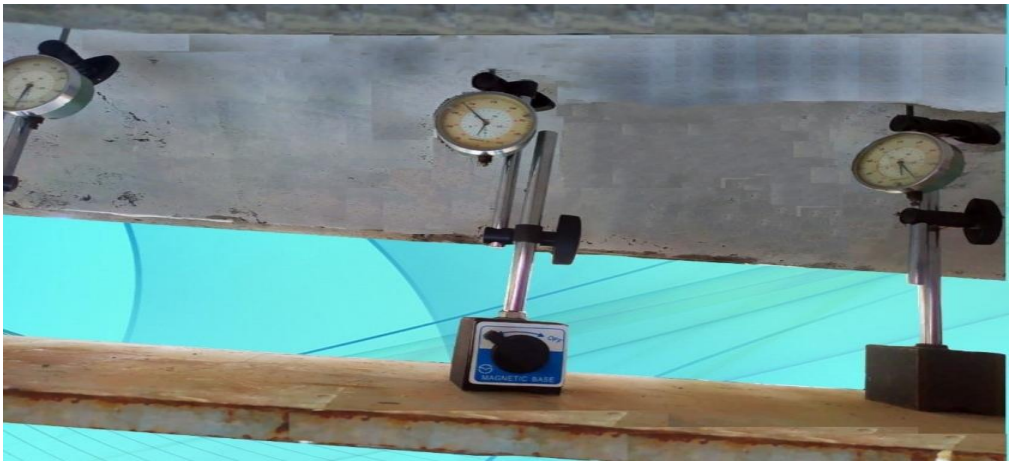

Fig. 14. Shows specimen during deflection measurement

Fig. 15. Shows specimen during the test

Fig. 16. Shows specimen during the test

Cracking Patterns and Mode of Failure Cracks were traced and marked throughout the side of the specimen. The first crack-load of each specimen, crack propagation, and failure mode were recorded. Flexural cracks developed near the mid-span of the specimen. With the increase of the load, the cracks propagated vertically and new flexural cracks were developed rapidly. The cracks started to propagate wider when the specimens approached their failure load. As the load increased, more cracks started to develop and the crack at midspan started to propagate vertically towards the top surface of the specimen, while most of the developed cracks did not continue propagating. This could be attributed to the effect of steel mesh in controlling the crack width. The cracks for all tested panels can be shown in Figs. (17-26).

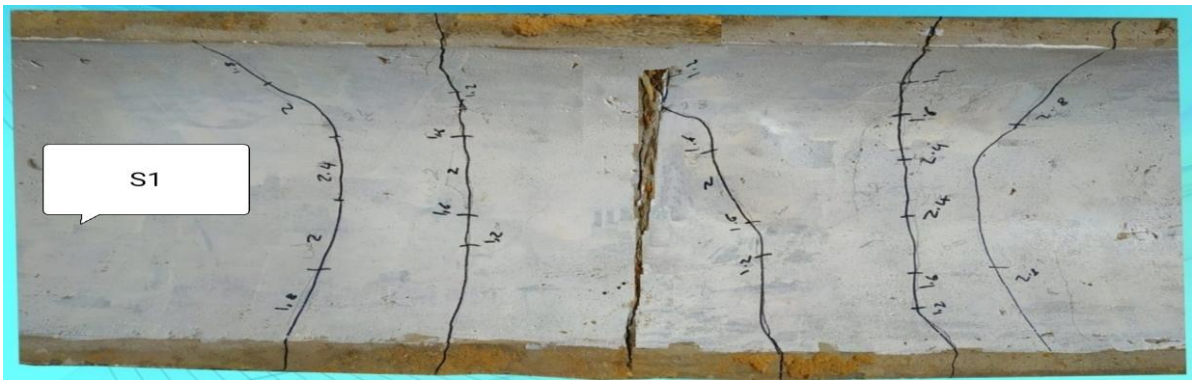

Fig. 17. Shows cracking shape of S1

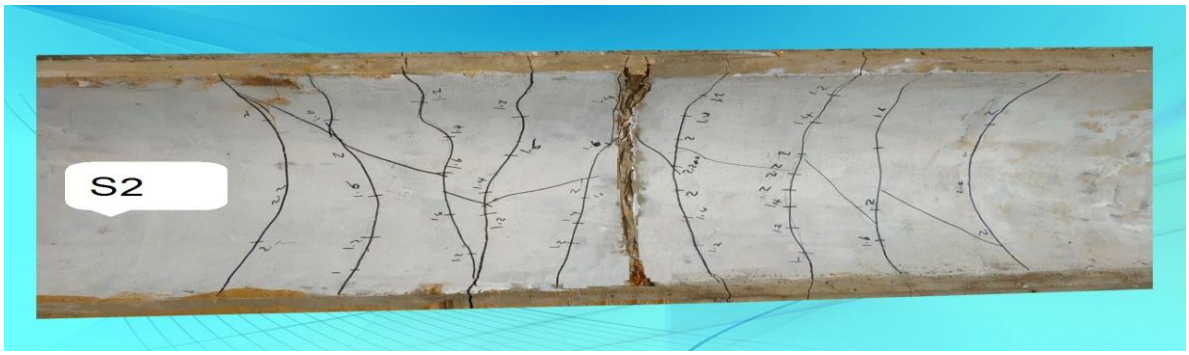

Fig. 18. Shows cracking shape of S2

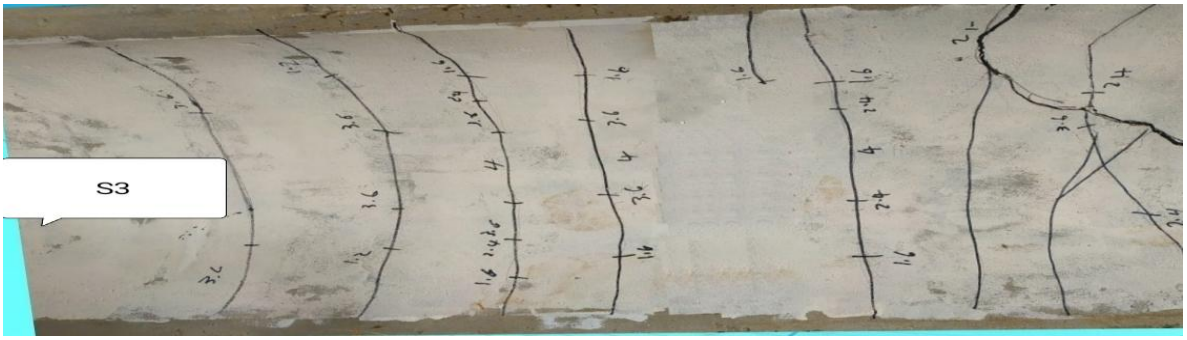

Fig. 19. Shows cracking shape of S3

Fig. 20. Shows cracking shape of S4

Fig. 21. Shows cracking shape of S5

Fig. 22. Shows cracking shape of S6

Fig. 23. Shows cracking shape of S7

Fig. 24. Shows cracking shape of S8

Fig. 25. Shows cracking shape of S9

Fig. 26. Shows cracking shape of S10

3. EXPERIMENTAL RESULTS

This section presents the experimental results of the test program and the discussion of the most important results. The results of the different test groups are compared to examine the effect of parameters on the structural responses of the proposed girders in terms of failure load, mode of failure, first crack load, service load, ductility ratio, and energy absorption were studied extensively. Fig. 27 presents: first crack, workability, Fig. 28 ultimate loads, Fig. 29. Failure load properties and Figure30. Failure load of all the tested girders. Load-Deflection Relationship as shown in Figs. (31-40) while Figs. (41-50) present relationship between load and strain.

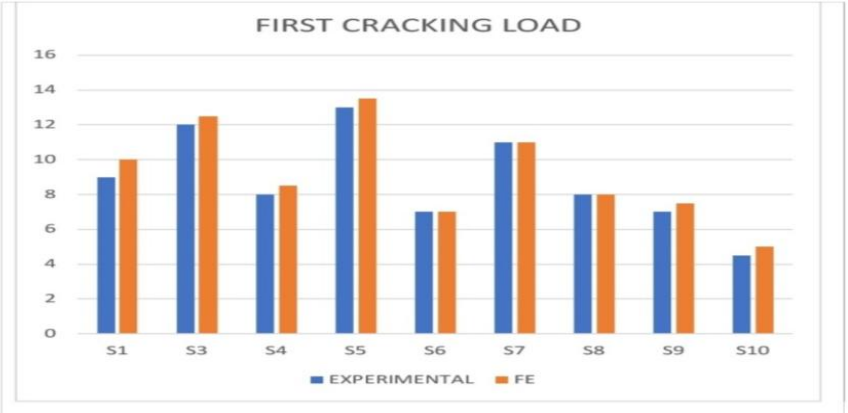

Fig. 27. First crack load and service load of all tested slabs

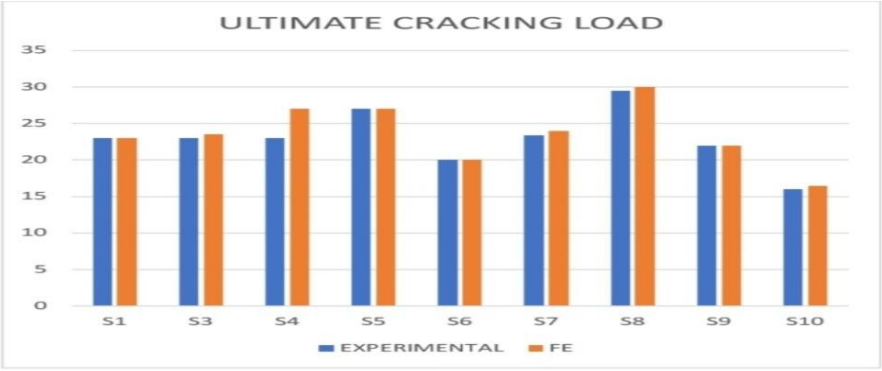

Fig. 28. Ultimate load of all tested panels

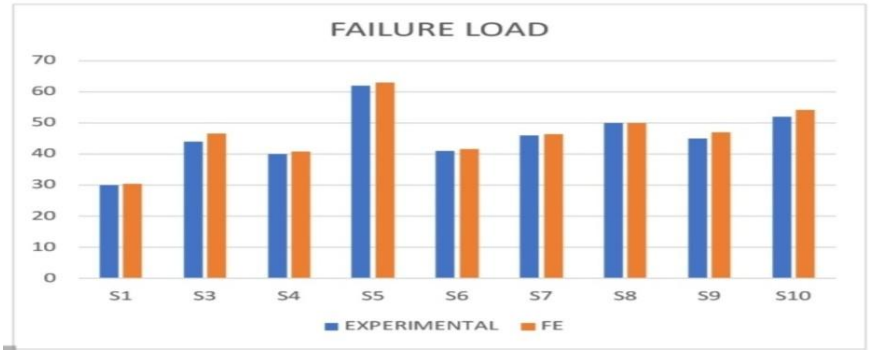

Fig. 29. Failure loads of all tested panels

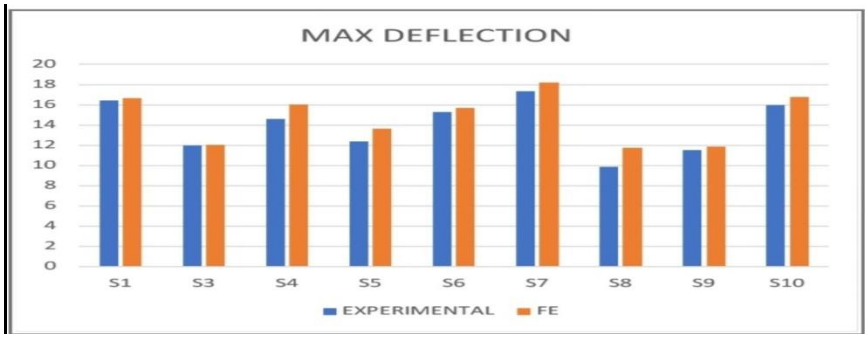

Fig. 30. Failure loads of all tested panels

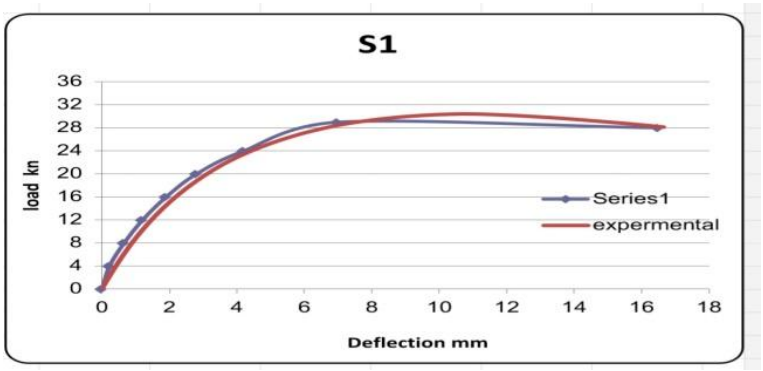

Fig. 31. Load- deflection curves for S1

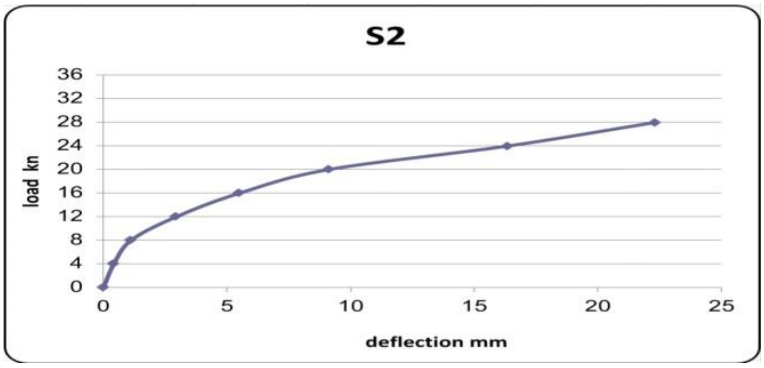

Fig. 32. Load- deflection curves for S2

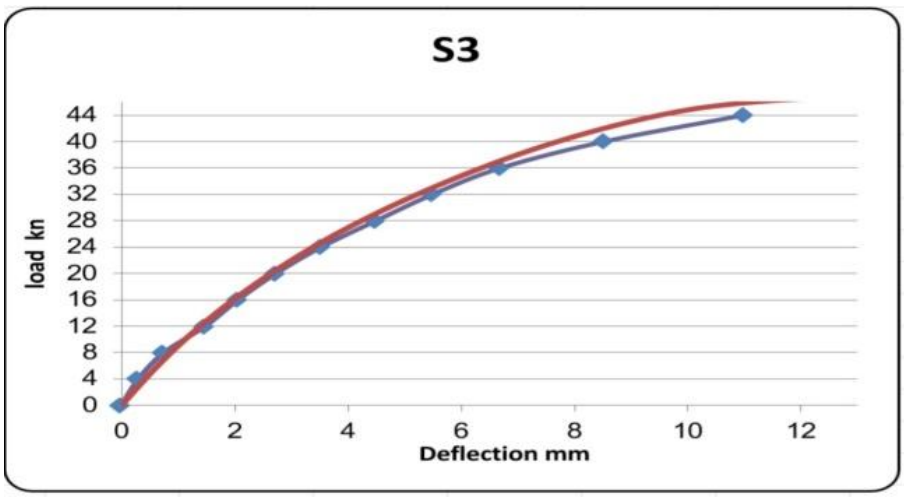

Fig. 33. Load- deflection curves for S3

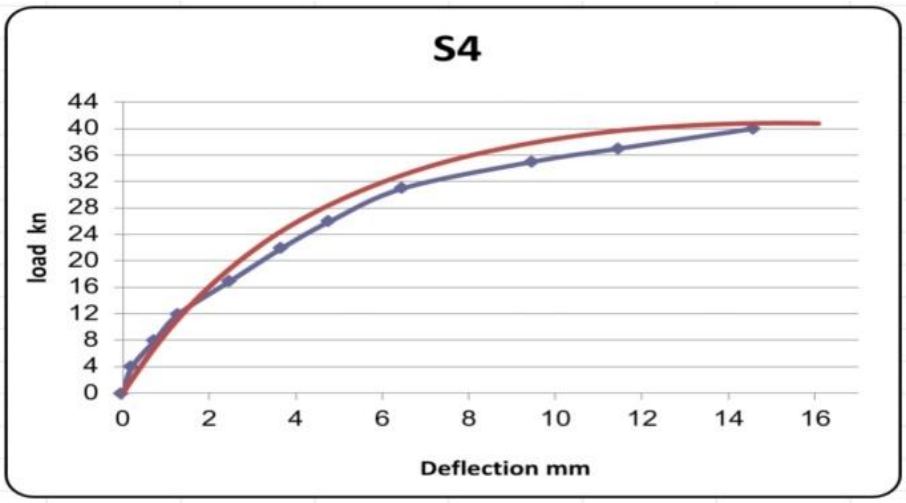

Fig. 34. Load- deflection curves for S4

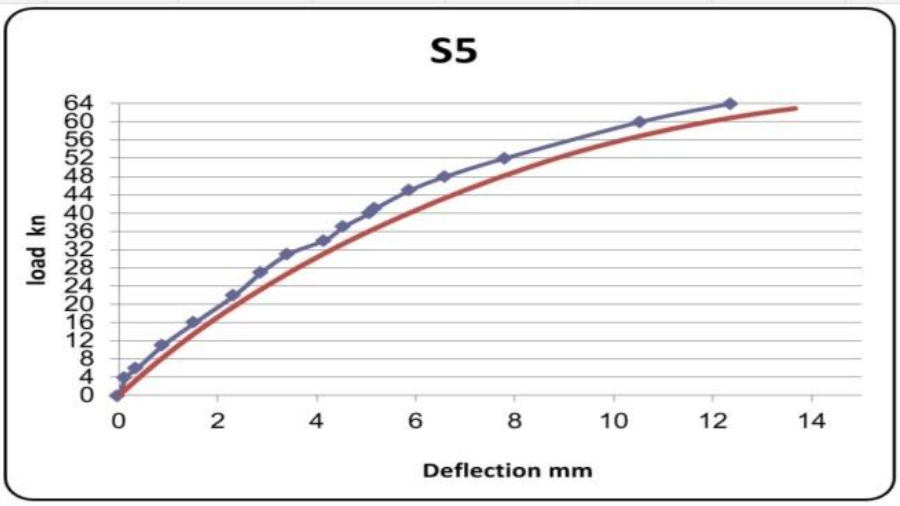

Fig. 35. Load- deflection curves for S5

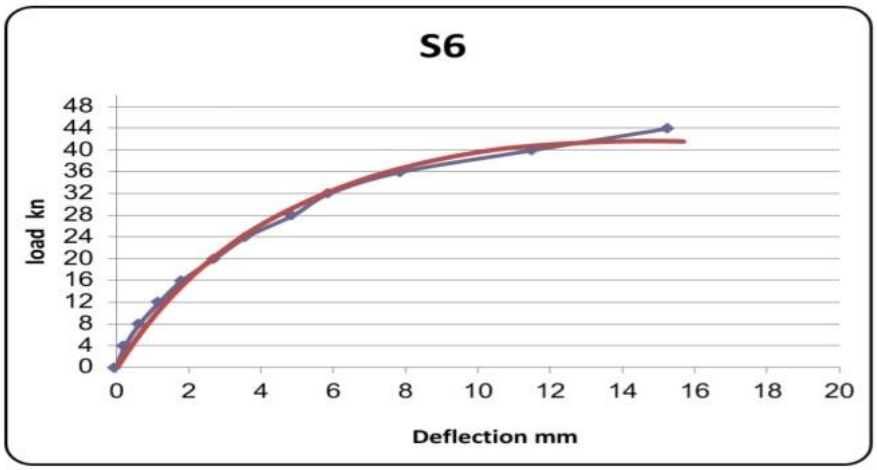

Fig. 36. Load- deflection curves for S6

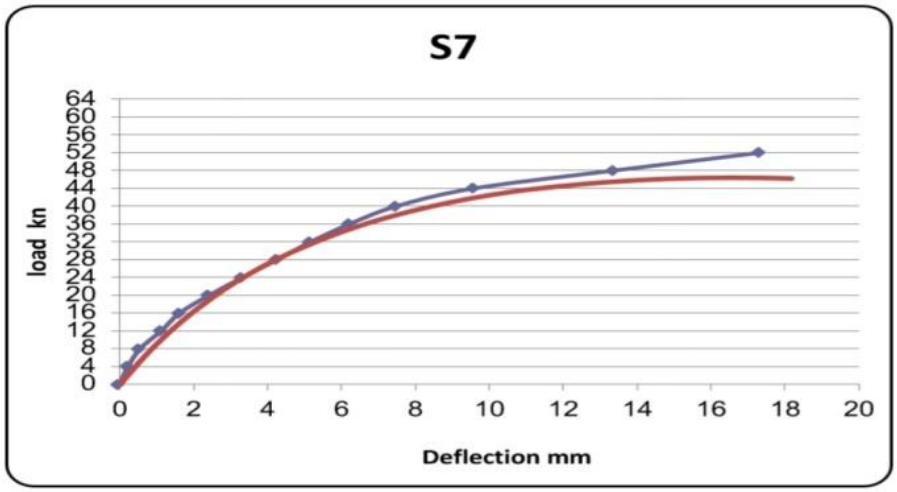

Fig. 37. Load- deflection curves for S7

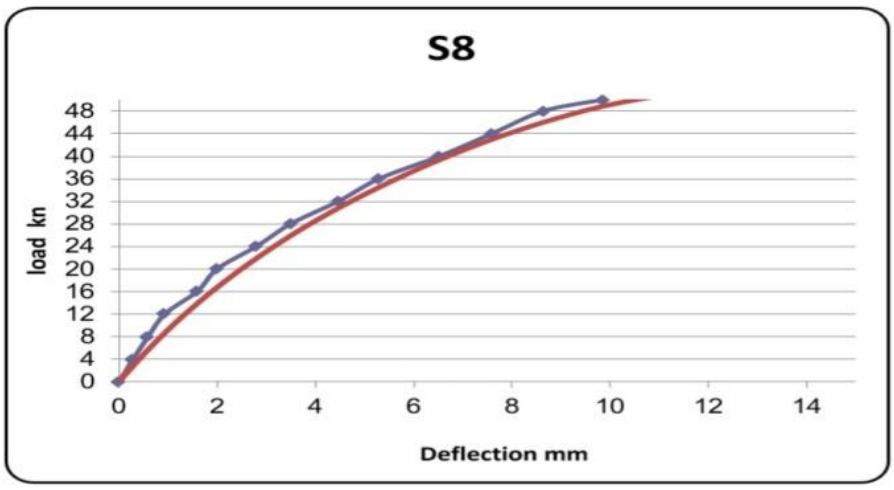

Fig. 38. Load- deflection curves for S8

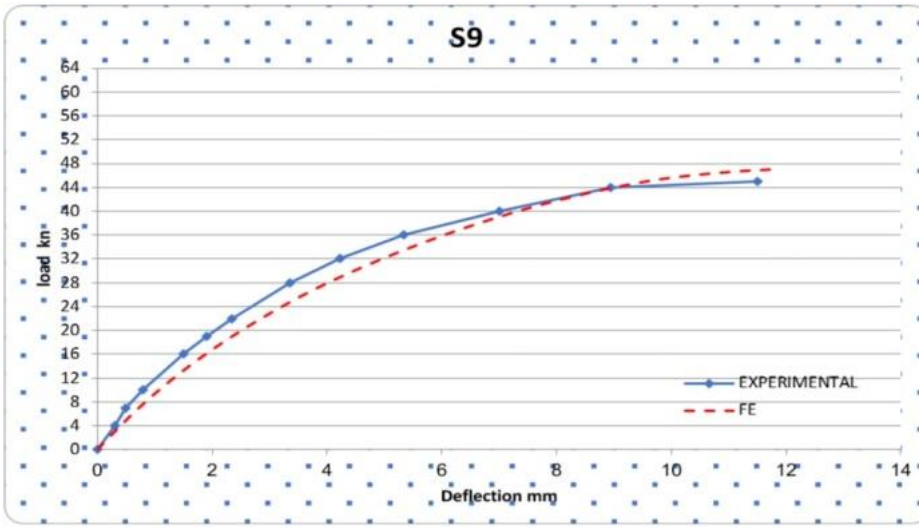

Fig. 39. Load- deflection curves for S9

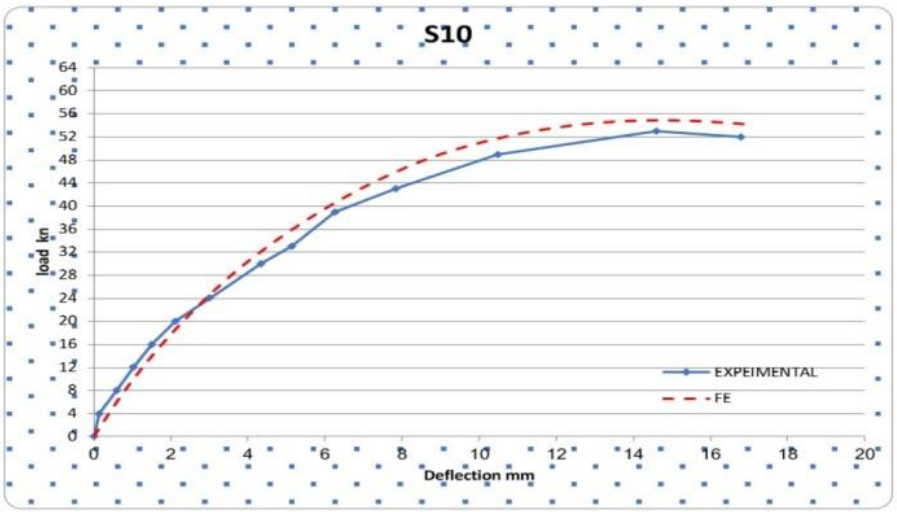

Fig. 40. Load- deflection curves for S10

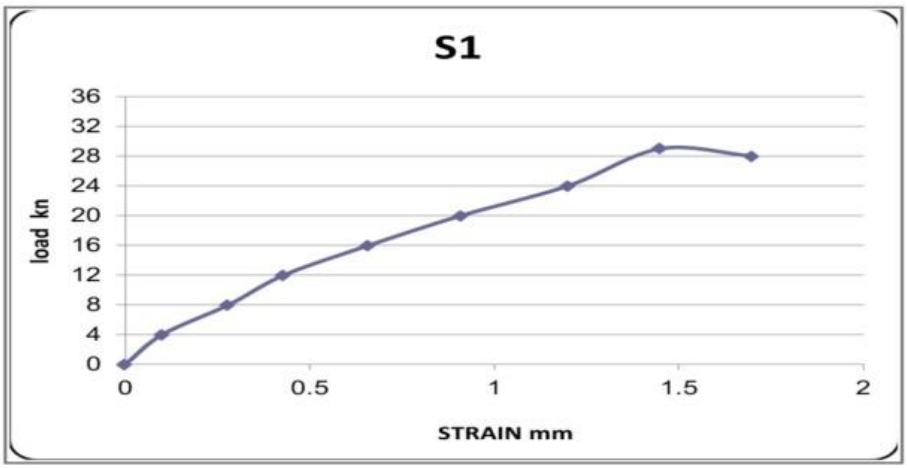

Fig. 41. Load- strain curves for S1

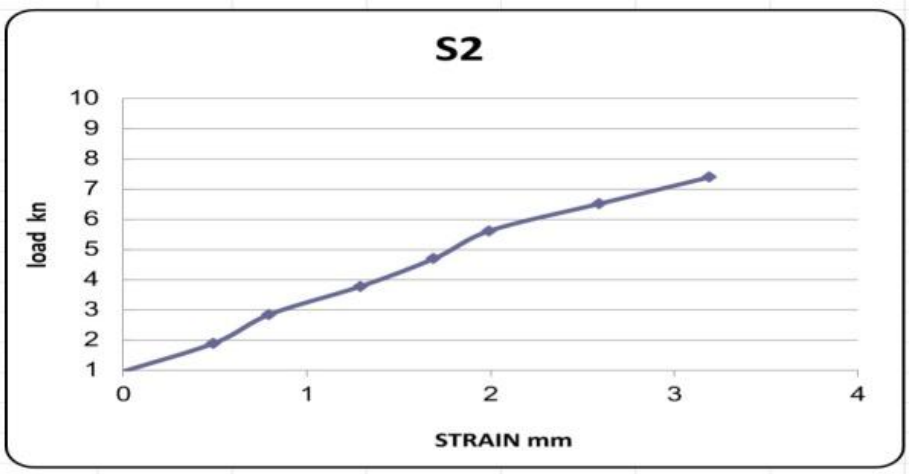

Fig. 42. Load- strain curves for S2

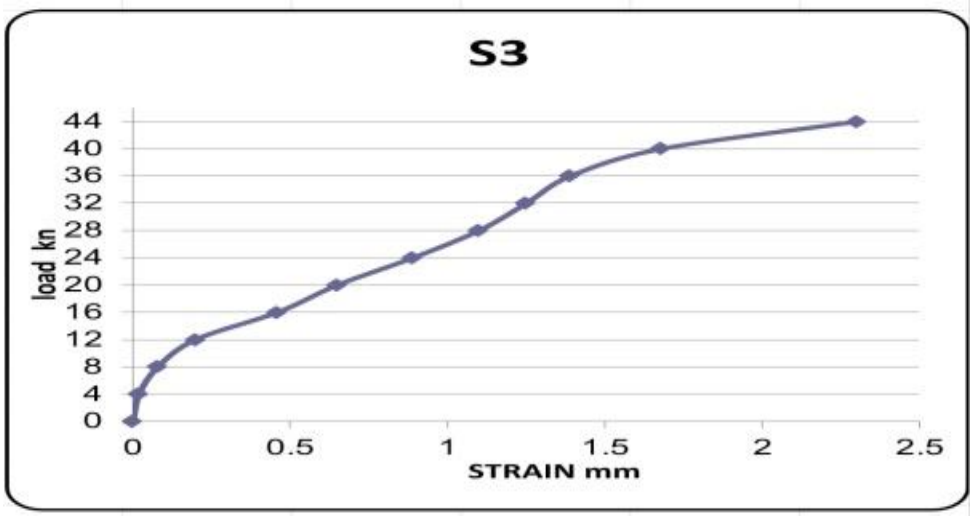

Fig. 43. Load- strain curves for S3

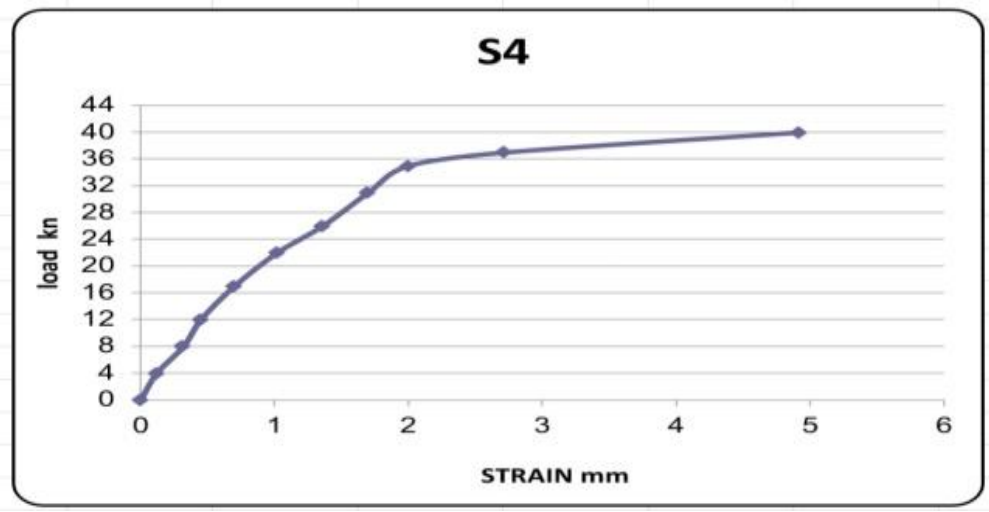

Fig. 44. Load- strain curves for S4

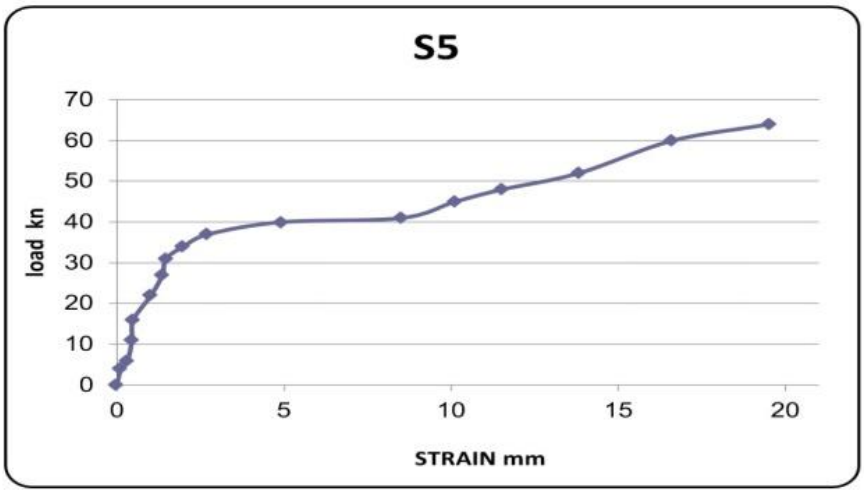

Fig. 45. Load- strain curves for S5

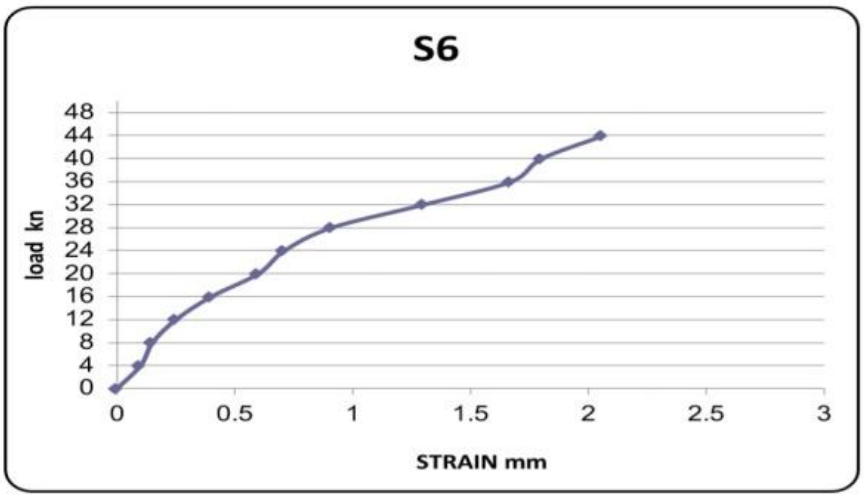

Fig. 46. Load- strain curves forS6

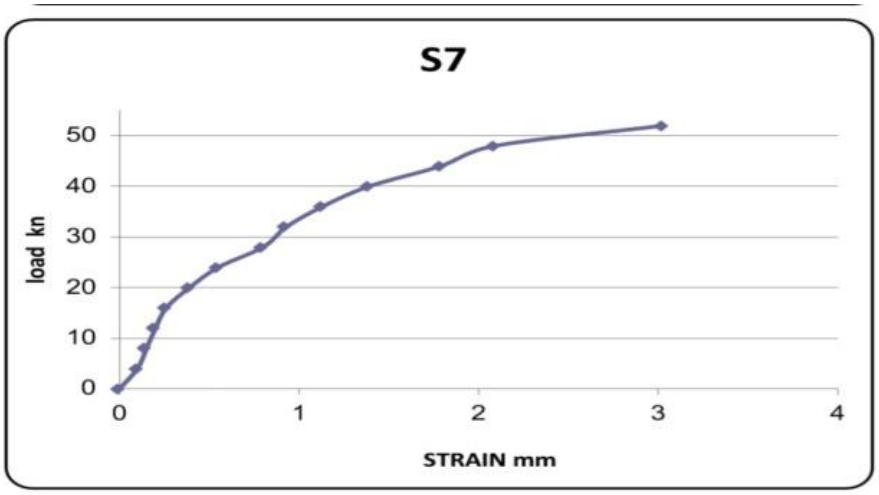

Fig. 47. Load- strain curves for S7

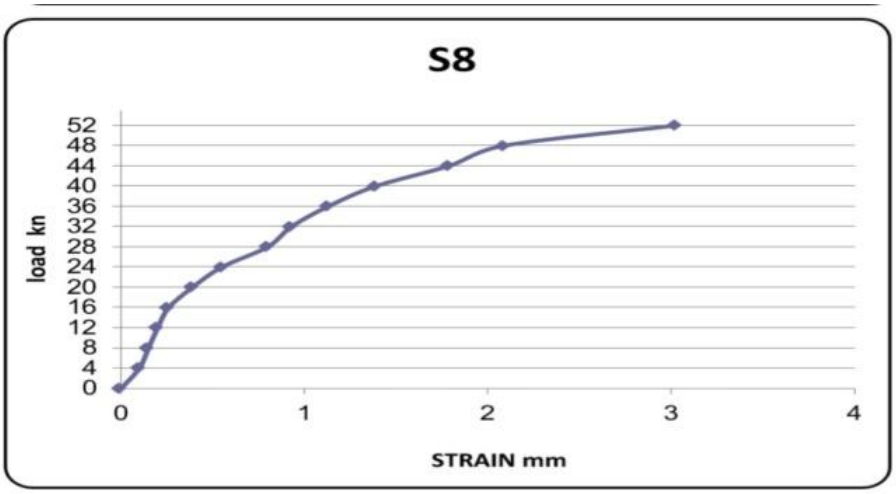

Fig. 48. Load- strain curves forS8

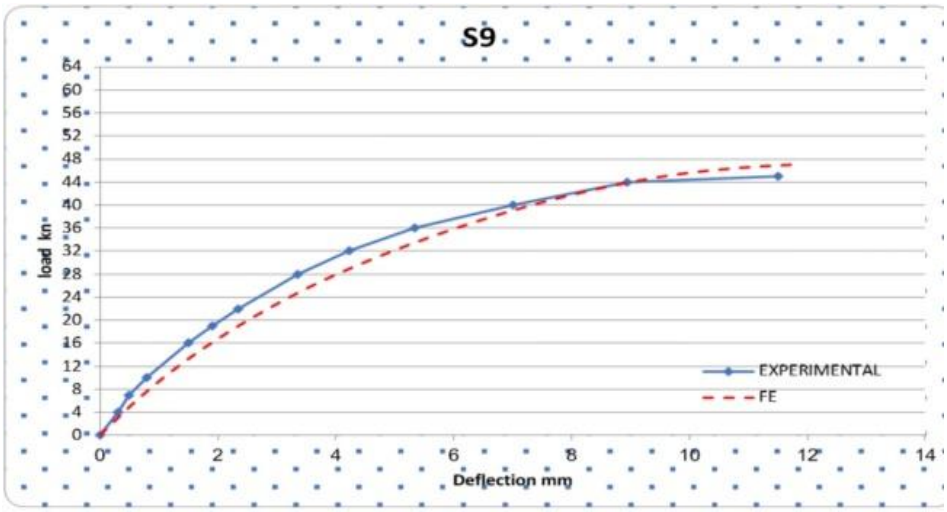

Fig. 49. Load- strain curves for S9

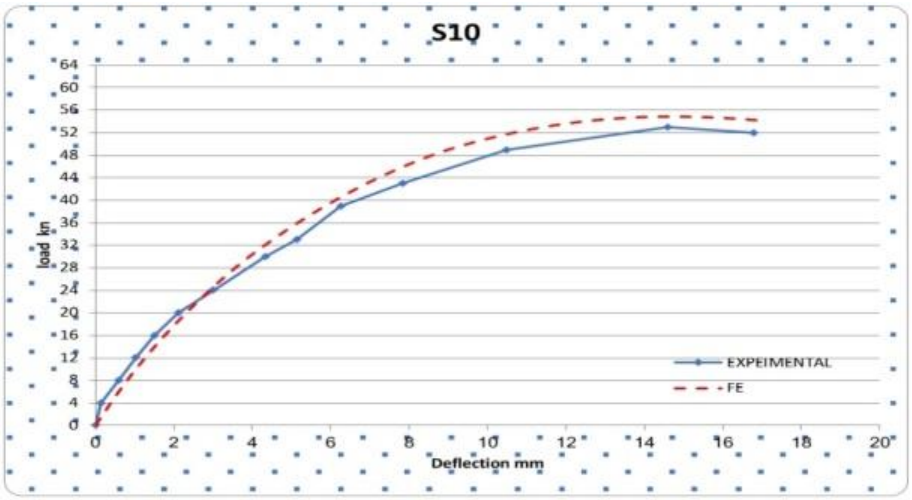

Fig. 50. Load- strain curves forS10

4. 1 Finite Element

simulation The specimens of study were modeled as 3D structures in Abaqus. Concrete parts were modeled using C3D8R. Steel bars, welded, expanded steel mesh and tenax mesh were modeled using T3D2 elements. Fig. 51 shows modeling of all parts (reinforced concrete, Steel bars, welded, expanded metal mesh, tenax mesh) in Abaqus. cracking pattern for panels from the theoretical for all specimens shown in Figs. (52-69).

4.2 Materials Modeling

4.2.1 Concrete

Concrete material was modeled using Abaqus concrete damage plasticity model. This model uses the concept of isotropic damage elasticity in combination with isotropic compression and tensile plasticity to model the inelastic behavior of concrete. Tables 7 and 8 present concrete elastic properties and concrete damaged plasticity model parameter used in analysis.

4.2.2 Steel reinforcement and metal meshes

Steel reinforcement has approximately linear elastic behavior when the steel stiffness introduced by the Young's or elastic modulus keeps constant at low strain magnitudes. At higher strain magnitudes, it begins to have nonlinear, inelastic behavior, which is referred to as plasticity. The plastic behavior of steel is described by its yield point and its post-yield hardening. The shift from elastic to plastic behavior occurs at a yield point on a material stress-strain curve. Table 9 shows the elastic properties of steel bars and metal mesh 19.

4.2.3 Tenax mesh (LBO 330)

Tenax mesh was modeled as biaxial Lumina material which has equivalent stress in both main directions (transverse and longitudinal directions) and also has the same fail stress in both directions.so it has isotropic and linear behavior only. Mesh thickness was 2.4 mm and modulus of elasticity (161.5 Mpa) and tensile density strength (94 N/mm2) at MD and (69.44 N/mm2) at TD. 3.3 Interaction: Steel bars, metal meshes and tenax were modeled as embedded region in the surrounding solid elements in the concrete arched slabs as shown in Fig. 51.

4.2.4 Boundary condition

The loads were modeled as pressure on contact area which was (90× 500 mm) for every load. The bottom surface of concrete arched slab was prevented from translation YZ directions and from rotation about XZ direction at the two lines of contact with underneath roller supports. Concrete slab was exposed to two concentrated loads at equivalent distance from supports line. Loads and boundary conditions were illustrated in Fig. 51.

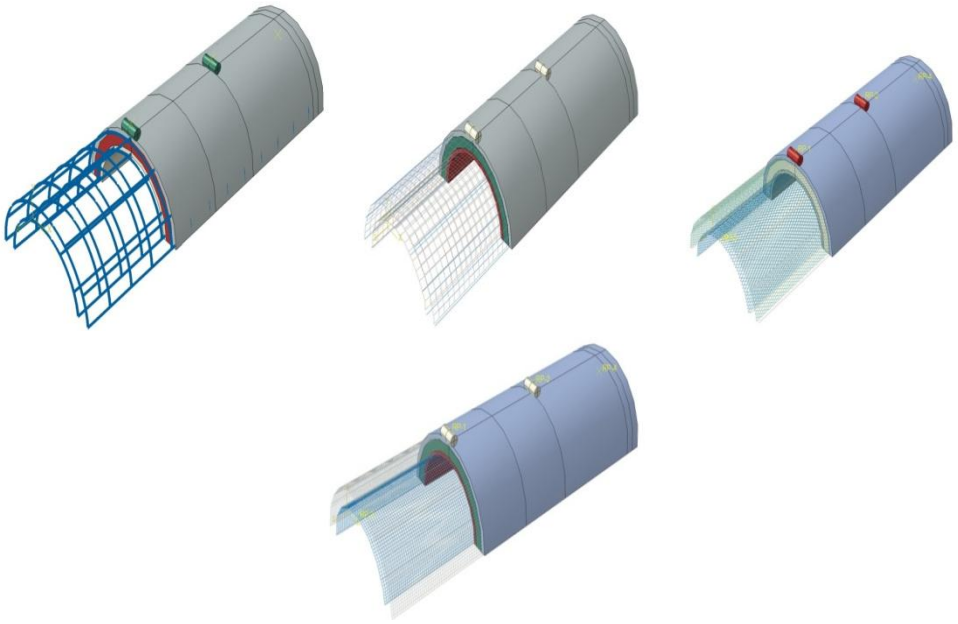

Fig. 51. Shows modeling of all parts

4.2.5 Meshing of model

The models were divided into fine elements with different sizes to allow quick analysis with sufficient accuracy. Total number of elements reached (374212) with sides varied .The fine element size was concentrated in region between applied loads.

5. COMPARISON BETWEEN EXPERIMENTAL AND FINITE ELEMENT SIMULATION RESULTS

The comparison between experimental and FE simulation. results ultimate load, 1st crack load, mid span deflection at the ultimate load are illustrated in Table 6. Fig. 27 and Fig. 28 present the applied load-mid span deflection, and the applied load-strain curves; respectively as obtained from the experimental and theoretical results for the all tested panels. The first crack load was determined as the first deviation from linearity of load deflection curve. The comparison between the experimental and theoretical cracking patterns for all tested specimens is presented in Fig. 29. Stresses distribution for all tested panels can be obtained at Fig. 30. Consequently, it can be concluded that the FE simulations give accurate results in comparing with the experimental results. In addition, these comparisons indicate a good agreement in slope of curves in the linear stage. For nonlinear stage, and due to the possibility of the inaccuracy in modeling the post yield behaviour of steel rebar material, there is somewhat none agreement between the finite element results and those of experimental results.

Table 7. Elastic properties of concrete

Parameter	Value
Density	2.4×10-9 N/mm3
Mod of elasticity	21900 MPa
Poissons ratio (v)	0.168

Table 8. Concrete plasticity parameters

Parameter	Value
Dilation angle	42
Eccentricity	0.11
Fb/fc	1.35
K	0.68
Viscosity parameter	0.0001
Yield stress n compression	17 MPA
Cross bonding inelastic strain	0.00
Compressive ultimate stress	33 MPA
Cross bonding inelastic strain	0.00158
Tensile failure stress	3.45MPA

Table 9. The elastic properties of steel bars and metal meshes

Steel 24/35		**Steel 36/52**		**Expanded mesh**		**Welded mesh**	
Density		Density		Density		Density	
7.8×10-9		7.8×10-9		7.8×10-9		7.8×10-9	
E	**Poissons ratio**	**E**	**Poissons ratio**	**E**	**Poissons ratio**	**E**	**Poissons ratio**
200000	0.3	210000	0.3	130000	0.28	170000	0.28
stress	strain	stress	strain	stress	strain	stress	strain
235.3596	0.00	353.0394	0.00	199	0.00	737	0.00
353.0394	0.0951	509.9458	0.0851	320	4.95E-02	834	0.05763

Table 6. Comparison between experimental and theoretical results

Specimens No.	First crack load(KN)			Ultimate load(KN)			Maximum deflection		
	Finite Element method results	Experimental study results	Percentage of difference	Finite Element method results	Experimental study results	Percentage of difference	Finite Element method results	Experimental study results	Percentage of difference
S1	10	9	1.11	23	23	1.00	16.5	16.3	1.01
S3	12.5	12	1.04	22	23.5	0.93	12	12	1.00
S4	8.5	8	1.06	27	23	1.17	16	14.7	1.08
S5	13.5	13	1.03	27.2	27.1	1.00	13.8	12.3	1.012
S6	6.9	7	0.98	20	20	1.00	15.8	15.5	1.01
S7	13.1	13	1.00	24	23.5	1.02	18	17.2	1.04
S8	8	8.2	0.97	30	29.5	1.01	11.9	10	1.19
S9	7.3	7	1.04	22	22.2	0.99	12	11.8	1.01
S10	5	4.6	1.08	16.5	16	1.03	17	16	1.06

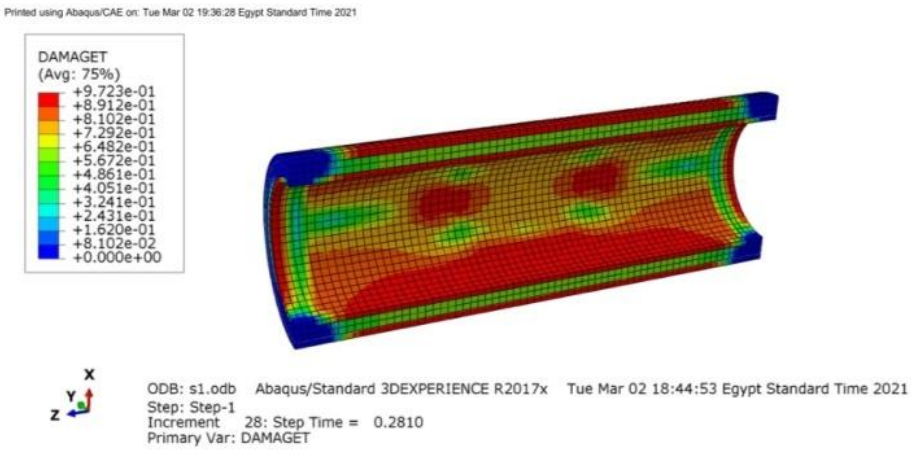

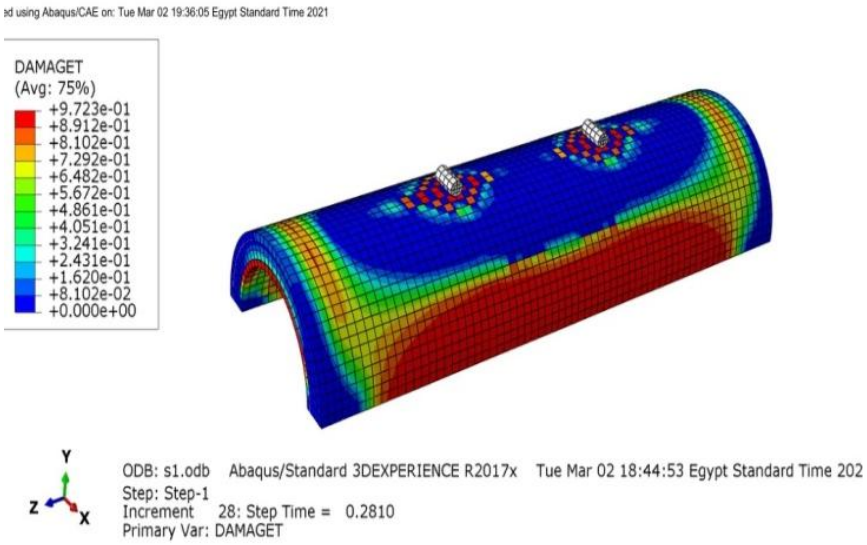

Figs. 52 and 53. Cracking pattern for panel S1 from the theoretical

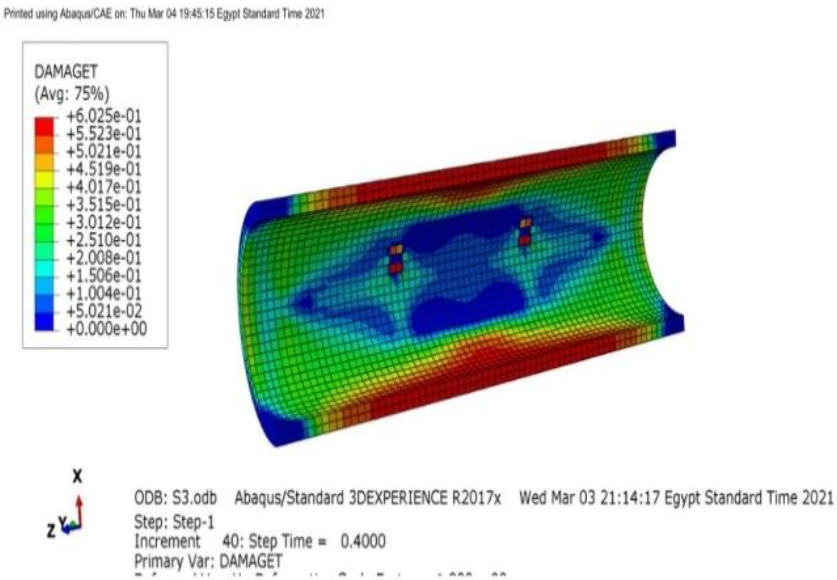

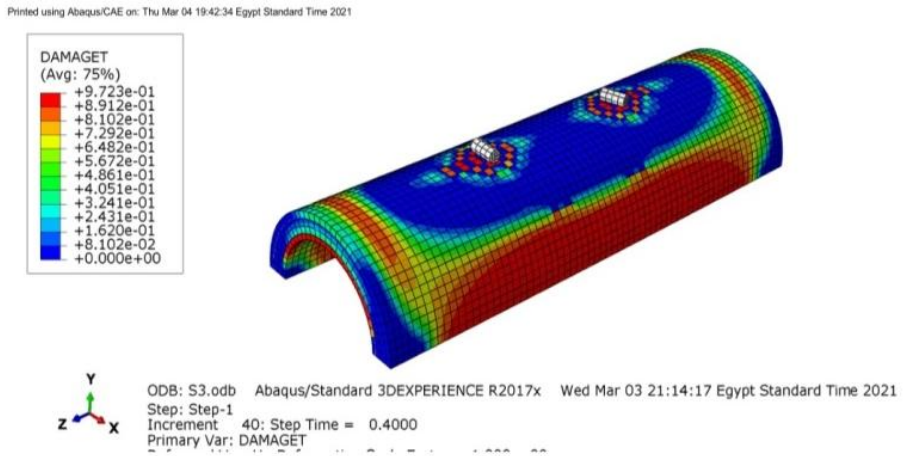

Figs. 54 and 55. Cracking pattern for panel S3 from the theoretical

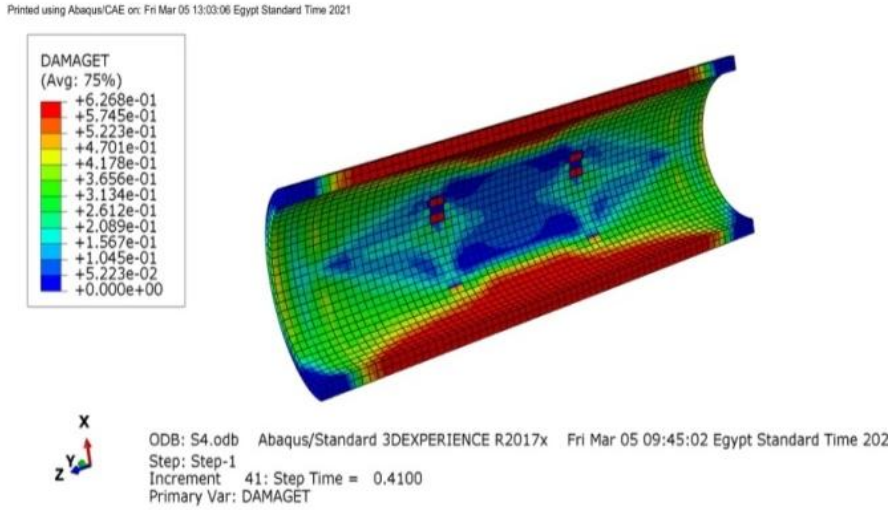

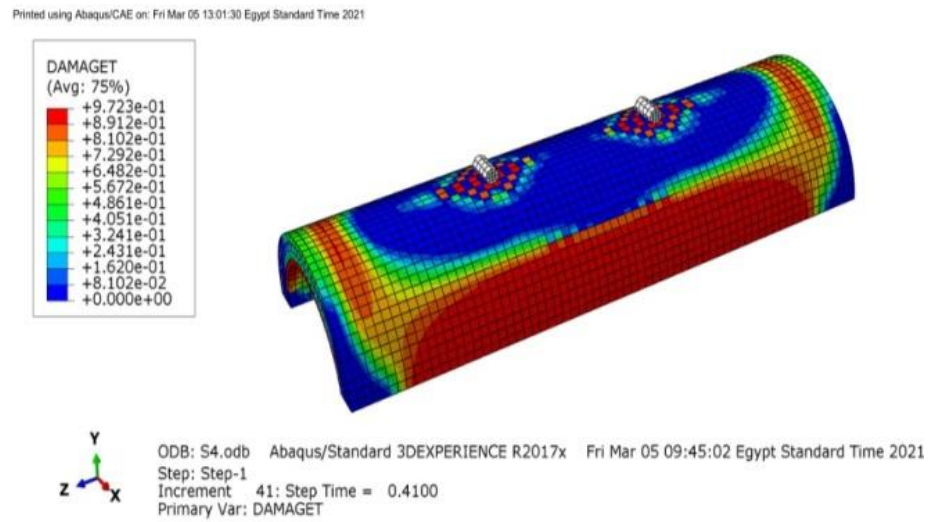

Figs. 56 and 57. Cracking pattern for panel S4 from the theoretical

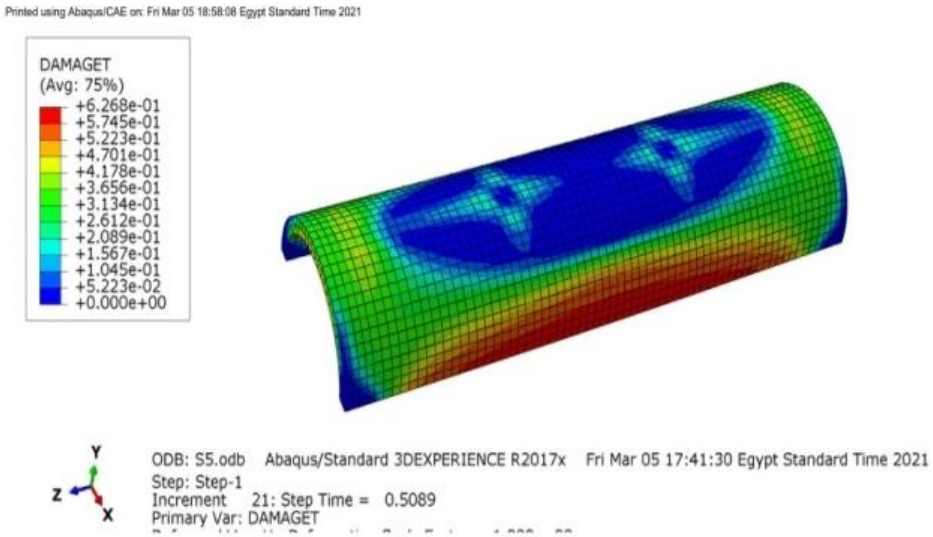

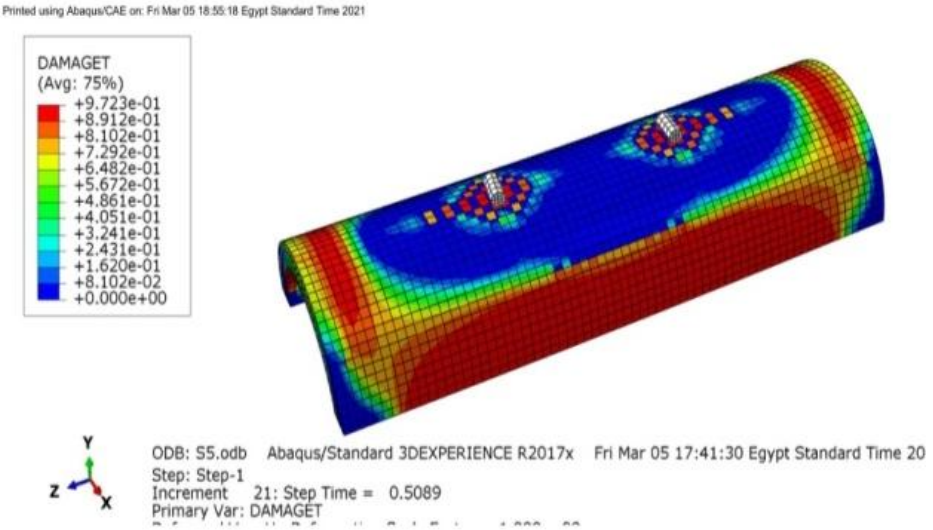

Figs. 58 and 59. Cracking pattern for panel S5 from the theoretical

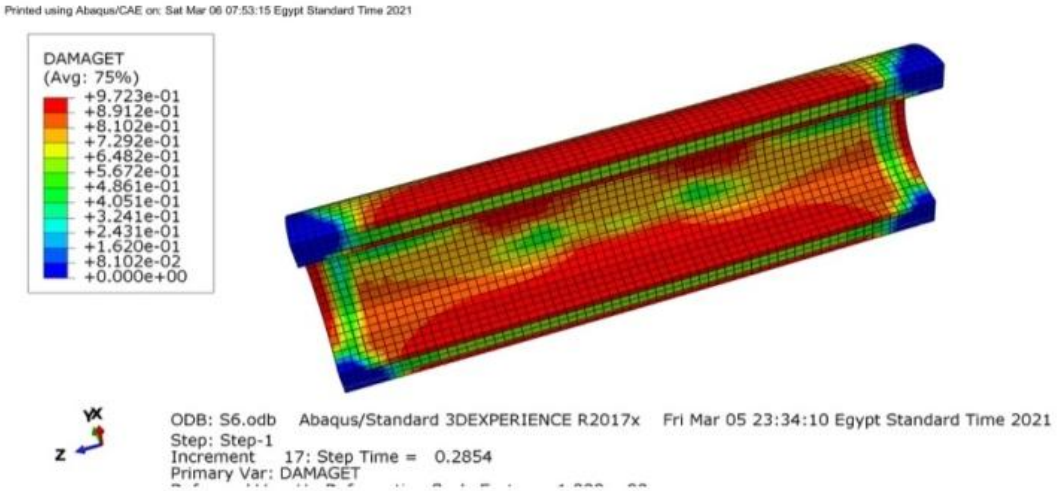

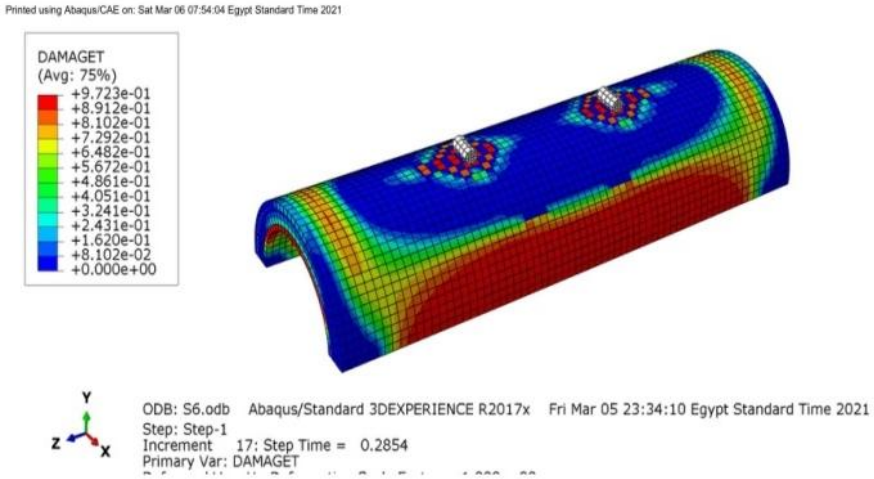

Figs. 60 and 61. Cracking pattern for panel S6 from the theoretical

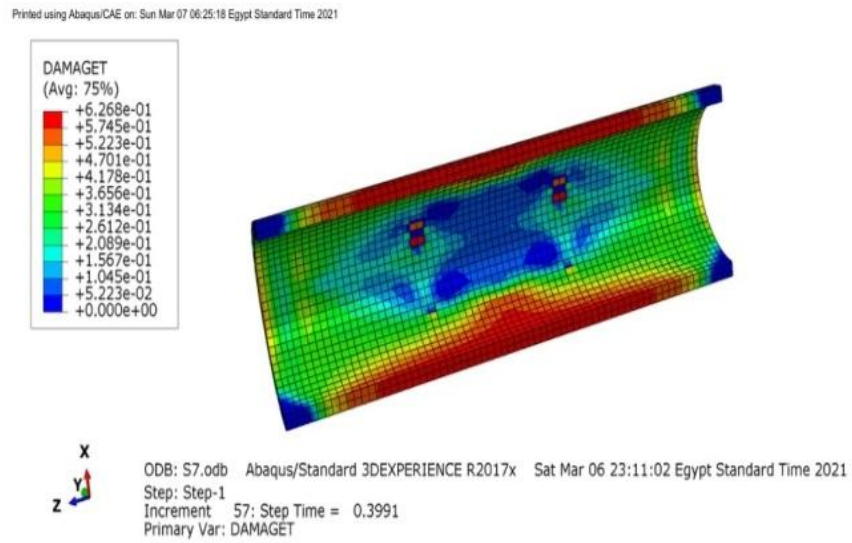

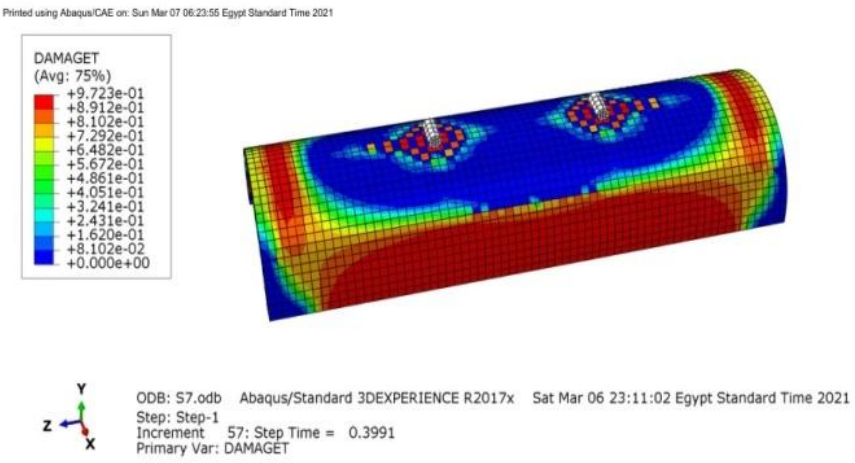

Figs. 62 and 63. Cracking pattern for panel S7 from the theoretical

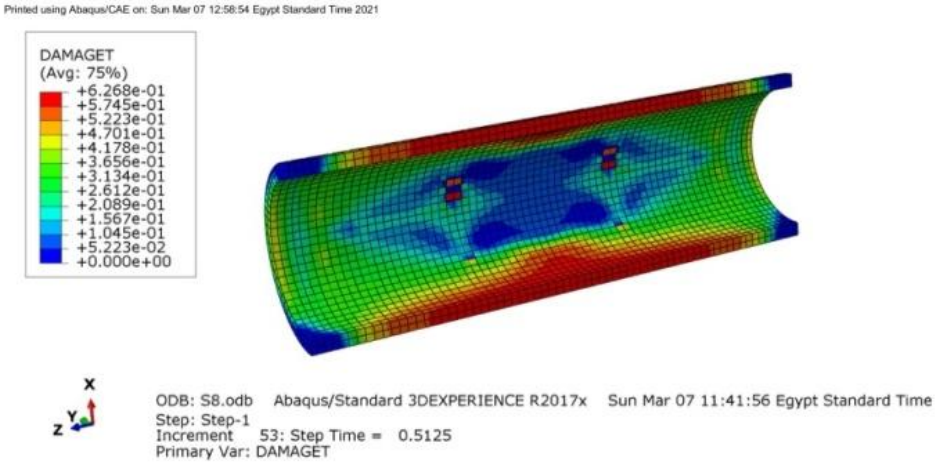

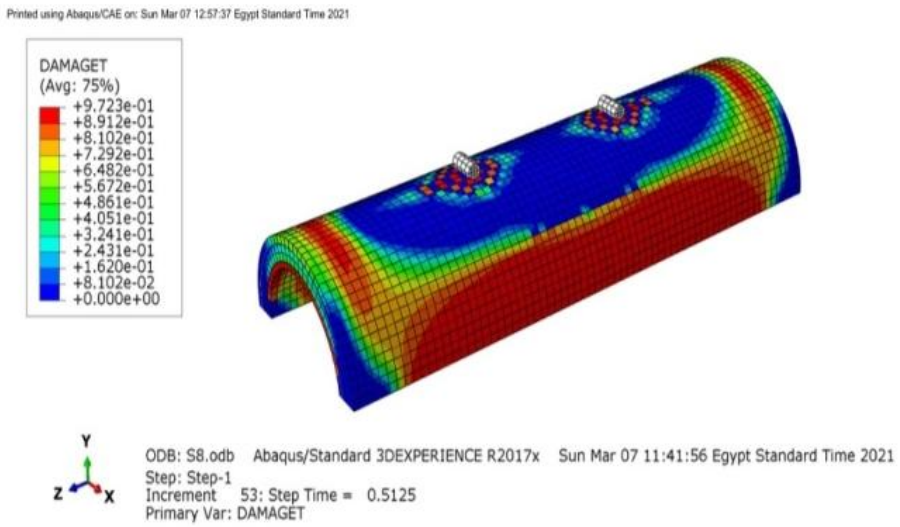

Figs. 64 and 65. Cracking pattern for panel S8 from the theoretical

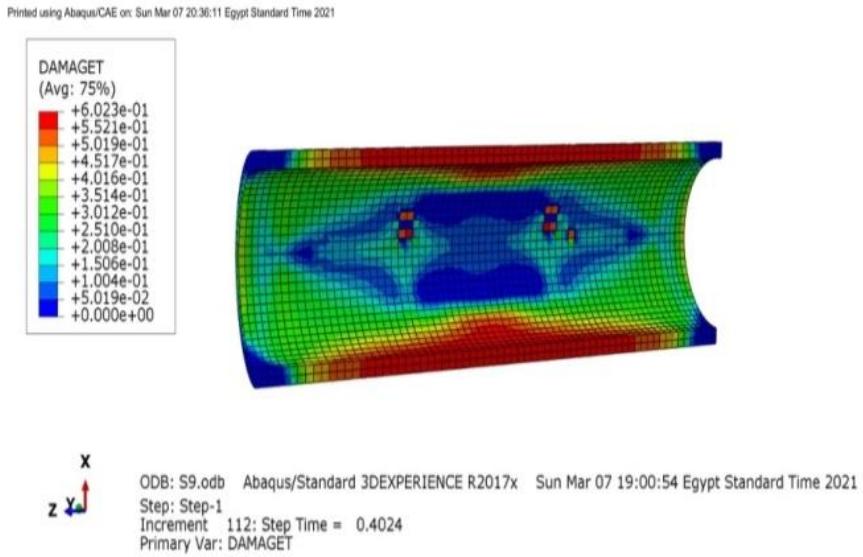

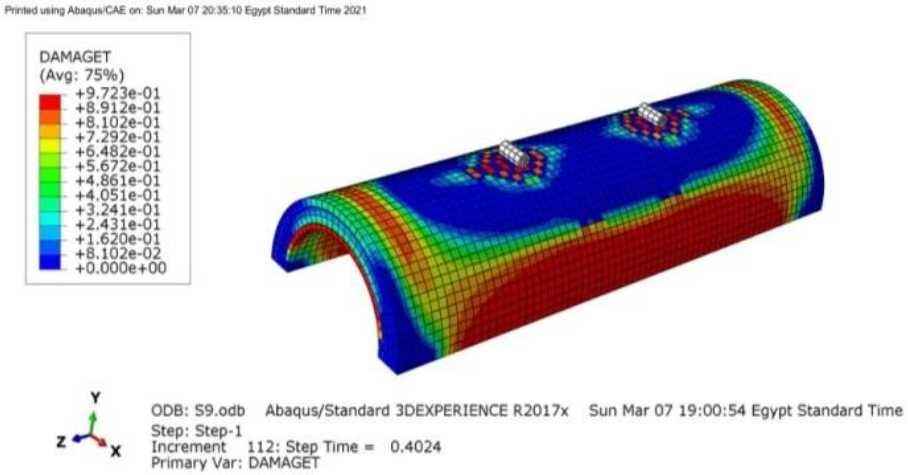

Figs. 66 and 67. Cracking pattern for panel S9 from the theoretical

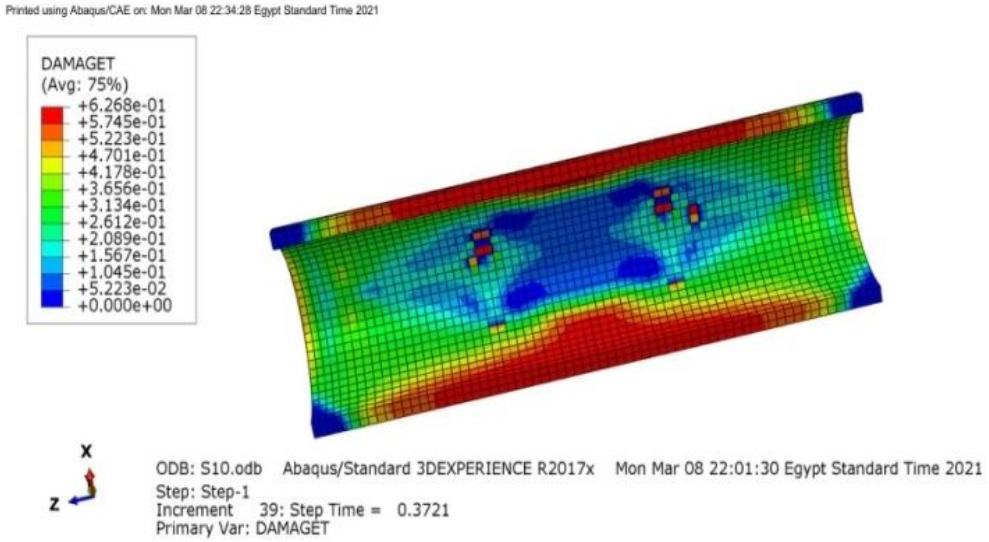

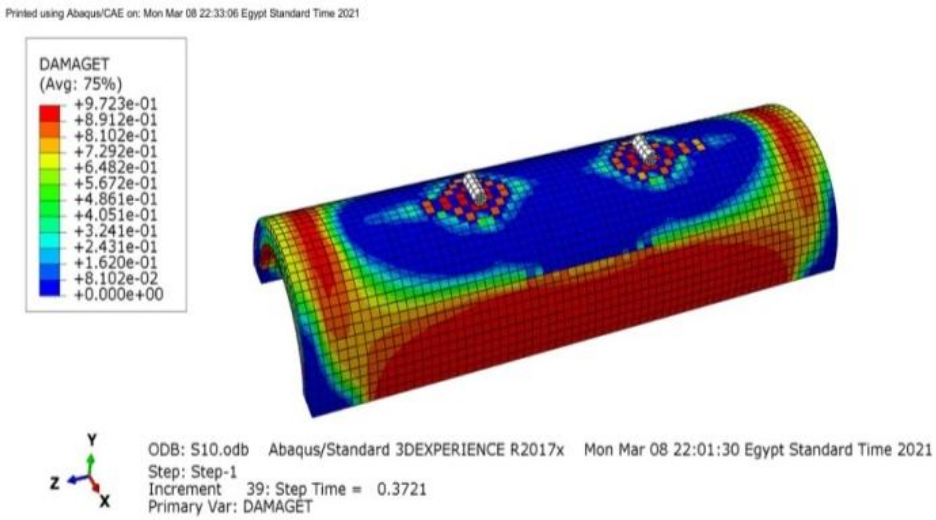

Fig. 68 and 69. Cracking pattern for panel S10 from the theoretical

6. CONCLUSION

The results also demonstrated that the presence of fibres in the mix improved the slab's overall performance. Within the scope, parameters, experimental investigation considered in this research and based on the test results and observations of the experimental investigation; the following conclusions and recommendations may be drawn as follows:

- Employing welded galvanized steel mesh gave the highest results compared to all tested semicircular tested slabs.
- Using polypropylene fibres in mortar mix increase in the first crack load, serviceability load, ultimate load, and energy absorption, higher stiffness However, less deflection at the corresponding load levels.
- Welded galvanized wire mesh achieved higher first crack load, serviceability load, ultimate load and energy absorption in comparison to reinforce with expanded and glass fibre meshes..
- Using (two-four) layers of welded galvanized steel mesh in reinforcing ferrocement slabs, improve the energy absorption than obtained when using skeletal steel bars.
- Using welded steel mesh with mild steel bars in reinforcing ferrocement slabs higher energy absorption than of using mild steel bars only. However the slabs showed less ductility ratio.
- Using five steel bars with one layer expanded metal mesh improve ductility ratio and energy absorption compared with using two-layer expanded metal mesh only.
- Increasing the number of the steel mesh layers in the ferrocement forms increases the first crack load, service load, ultimate load, and energy absorption.
- Using welded steel wire mesh reinforcement decreased the ductility ratio compared to that reinforced with glass fibre mesh and expanded steel mesh.
- The ductility ratio reduced. The percentage of reduction depends on the type and number of steel mesh layers in the ferrocement forms.

COMPETING INTERESTS

Authors have declared that no competing interests exist.

REFERENCES

1. ACI 549R-97, State-of-the-Art Report on Ferrocement, American Concrete Institute, Detroit, MI 48219, USA; 2009.
2. Shaheen YB, Eltehawy EA. Structural behaviour of ferrocement channels slabs for low cost housing. Challenge J. Concr. Res. Lett. 2017;8(2):48-64.
3. Shaheen Y, Eltaly B, Abdul-Fataha S. Structural performance of ferrocement beams reinforced with composite materials‖, Struct. Eng. 2014;50(6):817-834.
4. Singh V, Bansal PP, Kumar M. Experimental studies on strength and ductility of ferrocement jacketed RC beam-column joints. International Journal of Civil and Structural Engineering. 2015;5(3):199-205.
5. Ramakrishnan K, Muthu D, Viveka S. An experimental investigation of flexural behaviour of ferrocement box beams using micro fillers. In Sustainable Practices and Innovations in Civil Engineering. 2020;87-96.
6. Abbass AA, Abid SR, Arna'ot FH, Al-Ameri RA, Özakça M. Flexural response of hollow high strength concrete beams considering different size reductions. In Structures. 2020;23:69-86.
7. Du W, Yang C, Wang C, Pan Y, Zhang H, Yuan W. Flexural Behavior of Polyvinyl Alcohol Fiber–Reinforced Ferrocement Cementitious Composite. Journal of Materials in Civil Engineering. 2021;33(4):04021040.
8. Naser FH, Al Mamoori AHN, Dhahir MK. Effect of using different types of reinforcement on the flexural behavior of ferrocement hollow core slabs embedding PVC pipes. Ain Shams Engineering Journal; 2020.
9. Yousry BI, Shaheen1a, Hala M Refat, Ashraf M Mahmoud. Structural behavior of concrete walls reinforced with ferrocement laminates, Structural Engineering and Mechanics. 2021;78(4):455-471.
10. Egyptian Standards Specification, E.S.S, 4756-11. Physical and mechanical properties examination of cement, part 1, Cairo; 2012.
11. ASTM C1116/C1116M—10a. Standard specification for fiber reinforced concrete. ASTM international, West Conshohocken, PA; 2015.
    Available:http://www.astm.org/

12. Abdul-Fataha S. Structural behavior of concrete beams reinforced with innovative materials (Doctoral dissertation, M. Sc. thesis, Minufiya University, Shebin El-Kom, Egypt); 2014.
13. Acma LMC, Dumpasan GC, Salva MLI, Mansaguiton MP, Supremo RP, Daquiado NFP. Flexural strength and ductility behavior of ferrocement I-beam. Mindanao Journal of Science and Technology. 2015;13.
14. Eskandari H, Madadi A. Investigation of ferrocement channels using experimental and finite element analysis. Engineering Science and Technology, an International Journal. 2015;18(4):769-775.
15. Dajun D. Ferrocement Structures in China,‖ Journal of Ferrocement. 1993; 23(3):213-224.

Peer-review history:
The peer review history for this paper can be accessed here:
https://www.sdiarticle4.com/review-history/73077